Investigation of the Pressure Wave and Hot Gas Kernel Induced by Low Energy Electrical Discharges

Stefan Essmann[a], Detlev Markus[a], and Ulrich Maas[b]
[a]Physikalisch-Technische Bundesanstalt, Braunschweig, Germany
[b]Karlsruhe Institute of Technology, Karlsruhe, Germany

1 Introduction

Electrical discharges are a common safety relevant ignition source. The processes governing the ignition by electrical discharges have been the subject of numerous experimental and numerical studies [1–5]. Many of these studies consider ignition in automotive or aerospace applications where typical ignition energies are in the mJ range. In the present study, we investigated discharges with energies ranging from 30 to 1000 µJ which is in the range of the minimum ignition energy (MIE) of many burnable gases; thus, this energy range is of concern to safety relevant applications.

When an electrical discharge occurs, the energy that was previously stored in the capacitor is discharged into a fairly small volume of gas. Eventually most of the energy goes into gas heating which occurs across several chemical pathways of plasma reactions, each having a different time scale. A substantial fraction of the heating, depending on the characteristics of the discharge, takes place within tens to hundreds of nanoseconds [6–9]. This leads to the formation of a roughly cylindrical kernel in the inter-electrode region where temperature and pressure are much higher than in the surrounding gas. This kernel rapidly expands and after several 100 ns a shock wave detaches from the kernel perimeter. Over the course of its propagation it decays into a sound wave or, more generally, a pressure wave. The radial location of both the pressure wave front and the kernel (pressure wave radius and kernel radius) at a certain instant reveals information about the discharge in reference to energy and energy density. The goal of this study is to characterise low energy discharges by utilising a combination of experimental and numerical techniques. We used schlieren imaging to measure the radii and compared these to data obtained with one-dimensional numerical simulations.

2 Experimental Setup

Low energy electrical discharges were generated in air at atmospheric pressure and $21.0 \pm 0.5\,^{\circ}$C ambient temperature between two tungsten electrodes 2.4 mm in diameter with rounded tips that were located in a cylindrical stainless steel vessel (140 mm diameter, 110 mm height). The electrode distance L_s was 0.5 to 1.5 mm. The discharge energy E_s can be approximated by the energy stored on the capacitor, $E_\mathrm{s} = \frac{1}{2}CU^2$, where C is the capacitance of the setup (including stray capacitance) and U is the

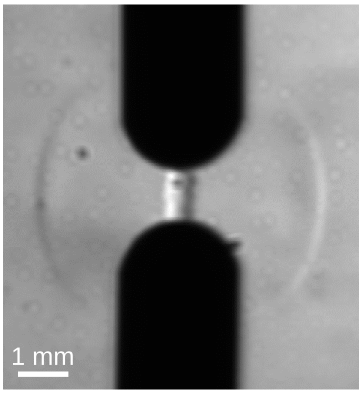

Figure 1: Schlieren image of the pressure wave and the kernel for case $L_s = 1.0\,\mathrm{mm}$, $E_s = 87.0\,\mu\mathrm{J}$, taken 6.70 µs after the discharge.

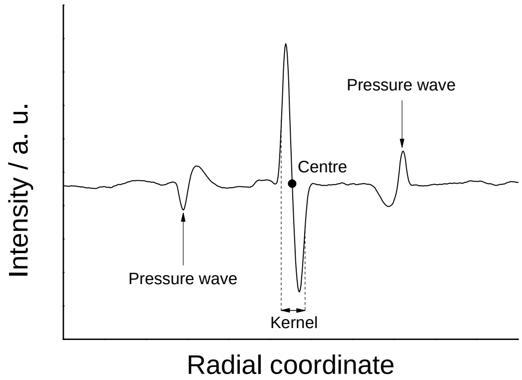

Figure 2: Intensity profile across radial coordinate (horizontal in fig. 1). The great peaks in the centre correspond to the hot gas kernel while the smaller ones relate to the pressure wave.

breakdown voltage. In order to achieve repeatable discharges, we slowly increased the voltage across the gap at $0.02\,\mathrm{kV\,s^{-1}}$ using a remote-controlled *FUG HCP 35-35000* high voltage source and an *Agilent 33500B* waveform generator. This yielded breakdown voltage variations smaller than 2 %. The discharge energy, calculated using the formula given above, scattered by less than 5 %.

Single shot images of the pressure wave and the hot gas kernel were taken using a schlieren setup. A *Nanolite KL-L* flashlamp which had a flash duration of less than 25 ns was used as a light source. The light from the flashlamp was focused onto a rectangular slit and then parallelised by a 500 mm collimating lens. Behind the vessel, it was focused by another 500 mm collimating lens and cut off using a knife edge. The images were taken by a *LaVision ImagerProPlus 2M* CCD camera with a spatial resolution of 54 pixel/mm. A *Yokogawa DL6154* oscilloscope recorded the discharge current, breakdown voltage and time of flashlamp trigger. The beginning of the discharge was identified by the rising current across the electrode gap. Since it was not known a priori when the discharge will occur, both the flashlamp and the camera were triggered by a *Quantum Composers Model 9500* delay generator which was triggered by the oscilloscope trigger out signal. The intrinsic delays of the camera and the flashlamp added to the chosen delay. Images could thus only be taken at times $t > 6.5\,\mu\mathrm{s}$ after the beginning of the discharge.

In order to assess the effects of discharge energy and energy density independently, we carried out measurement for (a) varying energies (energy ratios 1 : 2 : 3.5 : 5 : 10) at two fixed electrode distances (0.5 mm and 1.0 mm), and (b) constant energy at varying electrode distances (0.5 to 1.5 mm). Three images were taken for each instant t after the discharge in every configuration to determine the repeatability of the measurements. Figure 1 shows a sample schlieren image of the heated gas kernel and the pressure wave. The images were processed by means of linear filtering and background subtraction. Then a horizontal intensity profile from halfway between the electrodes was extracted from which the centre point as well as the positions of the kernel and the pressure wave were determined (fig. 2).

3 Numerical Simulation

A one-dimensional description of a spark discharge in air is used in this work. The spark channel is represented by means of a cylindrical geometry which is in good agreement with the experimental results as can be seen in fig. 1. Therefore, the spark is described as an infinite cylinder with radius r_s and the simulations were performed perpendicular to the spark channel. The solutions to the well-known mass, species, momentum, and energy equations were obtained using a time integration method implementing detailed transport models. All details concerning the numerical model are given in [10].

The initial conditions for the calculations were those of a quiescent, homogeneous air mixture. The boundary conditions were zero gradients at the inner boundary. The vessel was represented numerically using a constant outer radius of 5 cm and a constant wall temperature. Plasma effects are neglected, hence, the numerical representation considers only the local heating of the gas inside the ignition volume using a source term q in the energy conservation equation. The energy deposition term is given by [11]

$$q = \begin{cases} \frac{D_s}{t_s} \exp\left(-\left(\frac{r}{r_s}\right)^8\right) & \text{for } 0 \le t \le t_s \\ 0 & \text{for } t > t_s \end{cases}, \tag{1}$$

where D_s represents the spark energy density deposited during the spark duration $t_s = 500\,\text{ns}$. It is given by $D_s = E_s / \left(L_s \cdot \pi r_s^2\right)$. Here, r_s represents the spark radius ($r_s = 200\,\mu\text{m}$ when not stated otherwise). Heat losses to the electrodes and plasma processes like the breakdown phase are not considered directly in this work. By using the experimentally given spark duration, spark channel length, and spark energy, the spark radius was varied to examine the kernel growth and pressure wave propagation which are yielded from the temporal evolution of the density profiles in relation to the experimental method described above.

4 Results and Discussion

For a constant electrode distance the development of the pressure wave and kernel radii depends strongly on the discharge energy (fig. 3). With increasing discharge energy the pressure wave radius at a given time also increases while the pressure wave travels at about the speed of sound in all cases. The kernel radius at a given time is also larger at greater discharge energy.

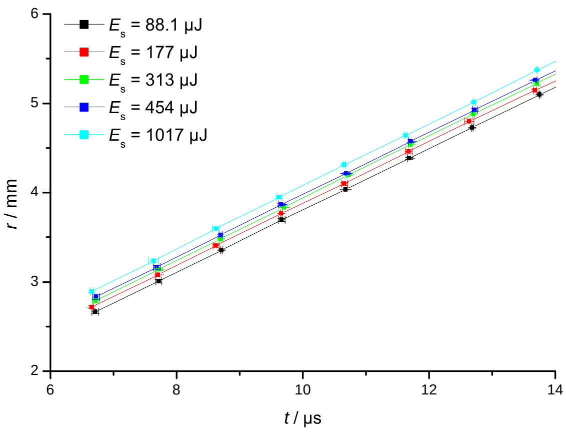

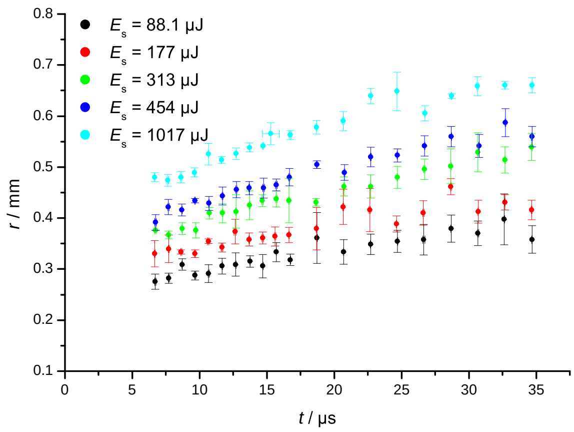

Figure 3: Experimentally determined pressure wave (left) and kernel (right) radii for $L_s = 1.0\,\text{mm}$. Each data point is an average of three realisations (error bars indicate their standard deviation).

Figure 4 (left) shows simulated radial locations for a fixed electrode distance. The trends are well captured in the simulation, as higher discharge energies yield greater pressure wave and kernel radii. A comparison of simulated kernel radial locations and experimentally determined kernel radii is shown in fig. 4 (right). While the general trend is reproduced, the simulation overestimates the kernel growth. This may be due to inefficient fast heating of the gas and losses in the experiment which are not considered

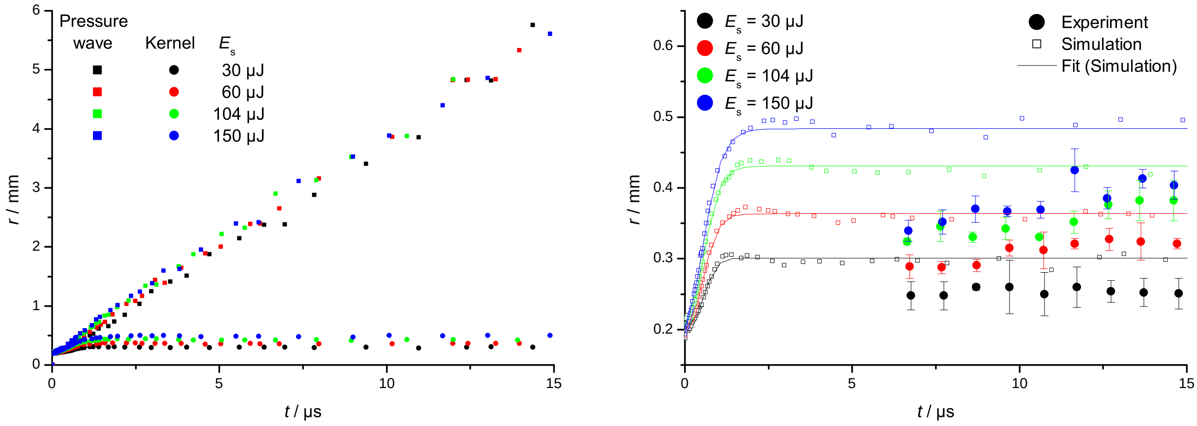

Figure 4: Simulated pressure wave and kernel radii (left), simulated kernel propagation and experimental kernel radii (right) for $L_s = 0.5\,\text{mm}$

by the simulation, or an incorrect initial spark radius r_s. Also, the slow growth of the kernel in the experiment is not captured in the simulation. Recirculation of the fluid at the electrode tips may be the cause [12]. Note that the shock wave detaches from the kernel within 1 µs in the simulation (fig. 4, left). The separation of the curves of different energies also takes place during the early stages.

This can be explained by taking a look at the simulated radial profiles of temperature, pressure, and density at different time steps for varying energies (fig. 5). The first two time steps up to about 500 ns show the heating of the gas due to the discharge. Here, the energy deposition term q is active. The temperature peaks at about 850 K and 3300 K in the low energy ($E_s = 30\,\mu\text{J}$) and high energy ($E_s = 150\,\mu\text{J}$) case, respectively. During these very first stages, there is a fast pressure rise. The pressure peak is much higher in the high energy case and, more importantly, is reached at an earlier time. The growth of the hot kernel is driven by pressure at these early times; the heat flux time scale is much larger. At high energy, the pressure in the centre already decreases at $t = 500\,\text{ns}$ due to the fast expansion of the kernel, whereas at lower energy it takes longer for the pressure in the centre to decrease. Hence, the kernel expansion which can best be monitored in the density profile is faster at high energy. The gradient of the pressure is steep enough to cause a shock wave to form. Detachment of the shock wave from the heated kernel can be seen after 700 to 1000 ns in the pressure and density profiles. It occurs earlier at high discharge energy which can also be seen in fig. 4 (left).

When the discharge energy is kept constant and the electrode distance is varied, no significant effect on pressure wave propagation is observed experimentally (fig. 6, left). The heated kernel radius, on the other hand, increases at smaller electrode distances. This is due to the fact that the energy density D_s increases when the gap becomes smaller. The same energy is discharged into a smaller volume and thus higher temperature and pressure result. The pressure wave radius apparently is not a function of energy density but only of energy. A possible explanation for this can be given when we investigate the effect of the spark radius r_s numerically (fig. 6, right). In these simulations, the energy and spark channel length were kept constant. The kernel growth rate is greater when r_s decreases, since the energy density is greater but the final kernel radius (after several µs) is still smaller than in cases with initially larger radii. Meanwhile, there is no trend concerning the pressure wave. The data shows that the shock wave detaches at an earlier time when the spark radius is small, thereby compensating for the initially smaller radius.

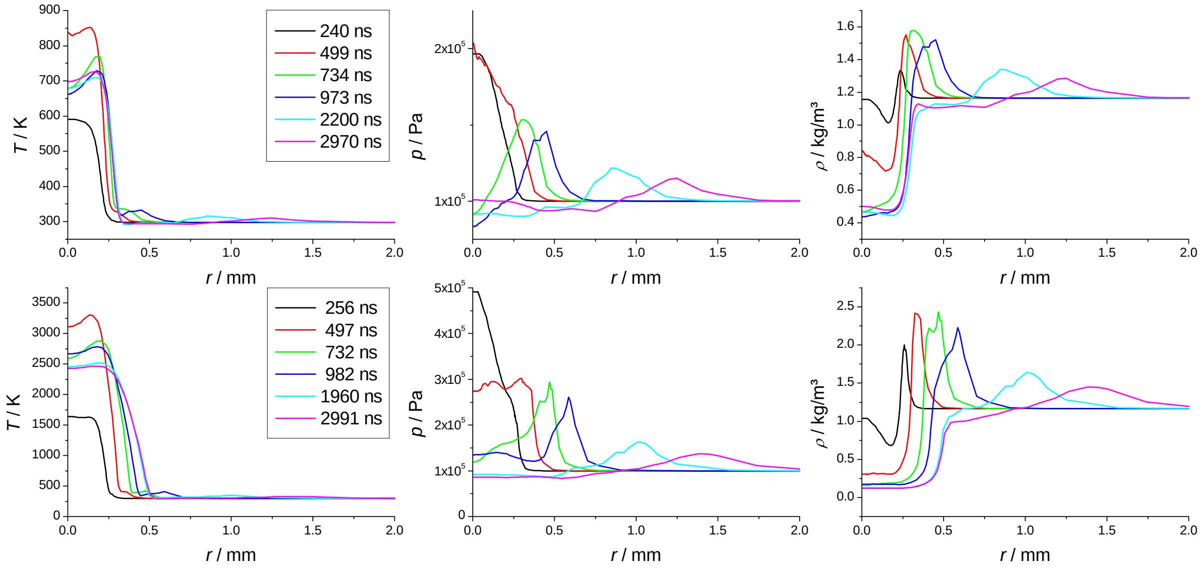

Figure 5: Radial profiles of temperature, pressure, and density (from left to right) for $L_s = 0.5\,\mathrm{mm}$ at two energies, $E_s = 30\,\mu\mathrm{J}$ (top row) and $E_s = 150\,\mu\mathrm{J}$ (bottom row), as functions of time.

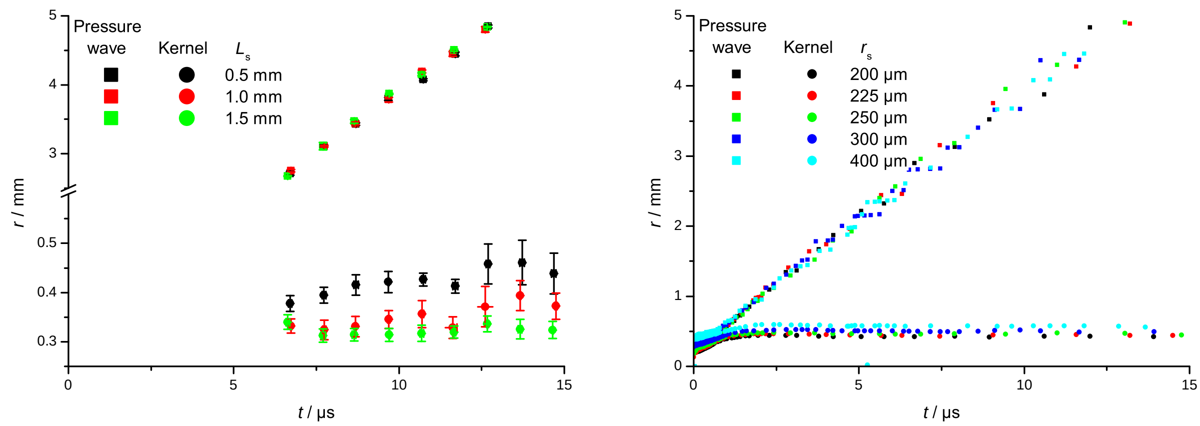

Figure 6: Experimentally determined pressure wave and kernel radii for $E_s = 240 \pm 10\,\mu\mathrm{J}$ (left), and influence of spark radius r_s on pressure wave and kernel for $L_s = 0.5\,\mathrm{mm}$, $E_s = 104\,\mu\mathrm{J}$ (Simulation, right).

5 Conclusion

The radial expansion of the pressure wave and kernel induced by low energy electrical discharges was measured in a phase resolved schlieren setup and was compared to one-dimensional numerical simulations. The pressure wave radius is a function of discharge energy and increases with increasing energy. The simulations showed that this is due to the faster expansion of the hot kernel at early times. In contrast, the kernel radius is a function of energy density. Increasing the spark radius in the simulation results in greater kernel radii but does not affect the radial location of the pressure wave at later instants.

While the qualitative agreement between experiment and simulation is good, more information about the early times is needed. Thus, in future work, we plan to change the experimental setup so earlier points in time will be accessible. Furthermore, a two-dimensional simulation could directly show the influence of spark channel length and consider fluid dynamic effects like recirculation at the electrode tips. Subsequently, using the correct initial spark radius r_s, we will be able to quantify the losses due to the shock wave, thermal losses, and other loss processes.

Acknowledgements

The authors would like to acknowledge funding from the Deutsche Forschungsgemeinschaft (DFG) under grant FOR1447.

References

[1] D. R. Lintin and E. R. Wooding, "Investigation of the ignition of a gas by an electric spark," *British Journal of Applied Physics*, vol. 10, no. 4, p. 159, 1959.

[2] R. Maly, "Ignition model for spark discharges and the early phase of flame front growth," *Symposium (International) on Combustion*, vol. 18, no. 1, pp. 1747–1754, 1981.

[3] D. Bradley and F. K.-K. Lung, "Spark ignition and the early stages of turbulent flame propagation," *Combustion and Flame*, vol. 69, no. 1, pp. 71–93, 1987.

[4] P. L. Pitt, R. M. Clements, and D. R. Topham, "The early phase of spark ignition," *Combustion Science and Technology*, vol. 78, no. 4-6, pp. 289–314, 1991.

[5] R. Ono, M. Nifuku, S. Fujiwara, S. Horiguchi, and T. Oda, "Gas temperature of capacitance spark discharge in air," *Journal of Applied Physics*, vol. 97, no. 12, p. 123307, 2005.

[6] N. A. Popov, "Investigation of the mechanism for rapid heating of nitrogen and air in gas discharges," *Plasma Physics Reports*, vol. 27, no. 10, pp. 886–896, 2001.

[7] N. L. Aleksandrov, S. V. Kindysheva, M. M. Nudnova, and A. Y. Starikovskiy, "Mechanism of ultra-fast heating in a non-equilibrium weakly ionized air discharge plasma in high electric fields," *Journal of Physics D: Applied Physics*, vol. 43, no. 25, p. 255201, 2010.

[8] D. L. Rusterholtz, D. A. Lacoste, G. D. Stancu, D. Z. Pai, and C. O. Laux, "Ultrafast heating and oxygen dissociation in atmospheric pressure air by nanosecond repetitively pulsed discharges," *Journal of Physics D: Applied Physics*, vol. 46, no. 46, p. 464010, 2013.

[9] D. A. Xu, M. N. Shneider, D. A. Lacoste, and C. O. Laux, "Thermal and hydrodynamic effects of nanosecond discharges in atmospheric pressure air," *Journal of Physics D: Applied Physics*, vol. 47, no. 23, p. 235202, 2014.

[10] U. Maas and J. Warnatz, "Ignition processes in hydrogen-oxygen mixtures," *Combustion and Flame*, vol. 74, no. 1, pp. 53–69, 1988.

[11] A. Dreizler, S. Lindenmaier, U. Maas, J. Hult, M. Aldén, and C. F. Kaminski, "Characterisation of a spark ignition system by planar laser-induced fluorescence of oh at high repetition rates and comparison with chemical kinetic calculations," *Applied Physics B: Lasers and Optics*, vol. 70, no. 2, pp. 287–294, 2000.

[12] S. P. Bane, J. L. Ziegler, and J. E. Shepherd, "Investigation of the effect of electrode geometry on spark ignition," *Combustion and Flame*, vol. 162, no. 2, pp. 462–469, 2015.